SUPPLEMENTARY INFORMATION:

S1: Cross-sectional intensity maps for different excitation conditions:

Figure S1 shows cross-sectional intensity maps showing the scattered field for illumination at four different conditions. These include: excitation of the system at the two resonance modes: (a,e) bonding and (d,h) anti-bonding resonance, (b,f) excitation close to the anti-bonding mode, and (c,g) excitation away from either resonance mode. From these plots, the relative enhancements for the various conditions can be compared, revealing a significantly high enhancement in the nanoring cavity when the bonding resonance mode is excited, compared to all the other cases. In fact, the scattered field corresponding to excitation of the anti-bonding resonance mode (especially in the ferrimagnetic film), is comparable to, or even slightly lower than, that for the case of off-resonance excitation. Hence for our magnetization dynamics experiments, we chose to compare only the cases corresponding to excitation of the bonding resonance mode (d,h) and for off-resonance excitation (c,g), since we do not expect a drastically different response between the cases of exciting the system at the anti-bonding resonance mode and exciting it off-resonance.

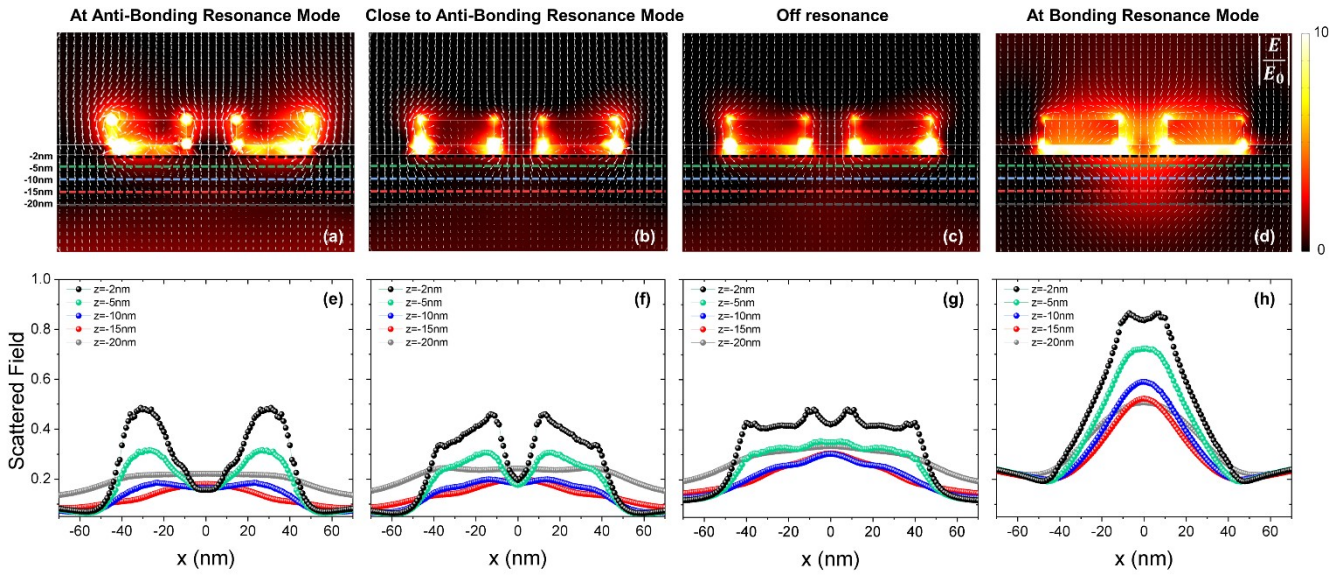

Figure S1. (Top) Cross-sectional plots of the near-field (E/E_0) for four excitation conditions as indicated above the maps: (a) at the anti-bonding Mode; (b) close to anti-bonding mode; (c) off-resonance (away from both modes) and (d) at the bonding resonance mode. The white arrows represent electric field flux lines. The dashed colour lines mark the distances from the Al_2O_3 (capping layer) -TbCo interface. (Bottom) Linear scans of the scattered field along the colored dashed lines in the top panels.

S2: Long timescale features of transmission and demagnetization traces:

Figure S2 shows the dynamics of our system at a longer time scale of up to 85 ps. For the magnetization dynamics corresponding to off-resonance excitation, at low fluence values, an ultrafast demagnetization is observed followed by recovery to the initial magnetic state. For higher fluences, the behaviour transitions into a three step demagnetization: two timescales are seen for demagnetization – an ultrafast sub-picosecond demagnetization followed by a slower demagnetization beyond 10 ps. An upturn is observed in the trace between 1 and 10 ps. Similar behaviour has been seen in GdFeCo and GdCo alloys[37], where the upturn has been attributed to a

heat-exchange between the two magnetic sublattices. Such a transition in the demagnetization behaviour with increasing fluence is not seen for on-resonance excitation even when nearly twice as much fluence is incident as compared to the high-fluence off-resonance excitation plotted in Figure S2. Rather the high-incident-fluence dynamics for resonant excitation remain similar to the low-fluence excitation dynamics seen for both cases, indicating that the effective fluence for resonant excitation might be much lower than the incident fluence. In the transmission dynamics, an oscillation can be seen in the first 20 ps, corresponding to excitation of a standing acoustic wave in the TbCo film. The frequency of the oscillation is the same for both on- and off-resonance excitation. From the time period of ~10 ps, and for our TbCo film thickness of 20 nm, the speed of sound v_s in TbCo can be extracted to be about 4000 m/s, which lies in the range of v_s observed in GdFeCo and TbFeCo alloys[38]. The increase in signal seen in Figure 3 of the main text is due to this standing wave.

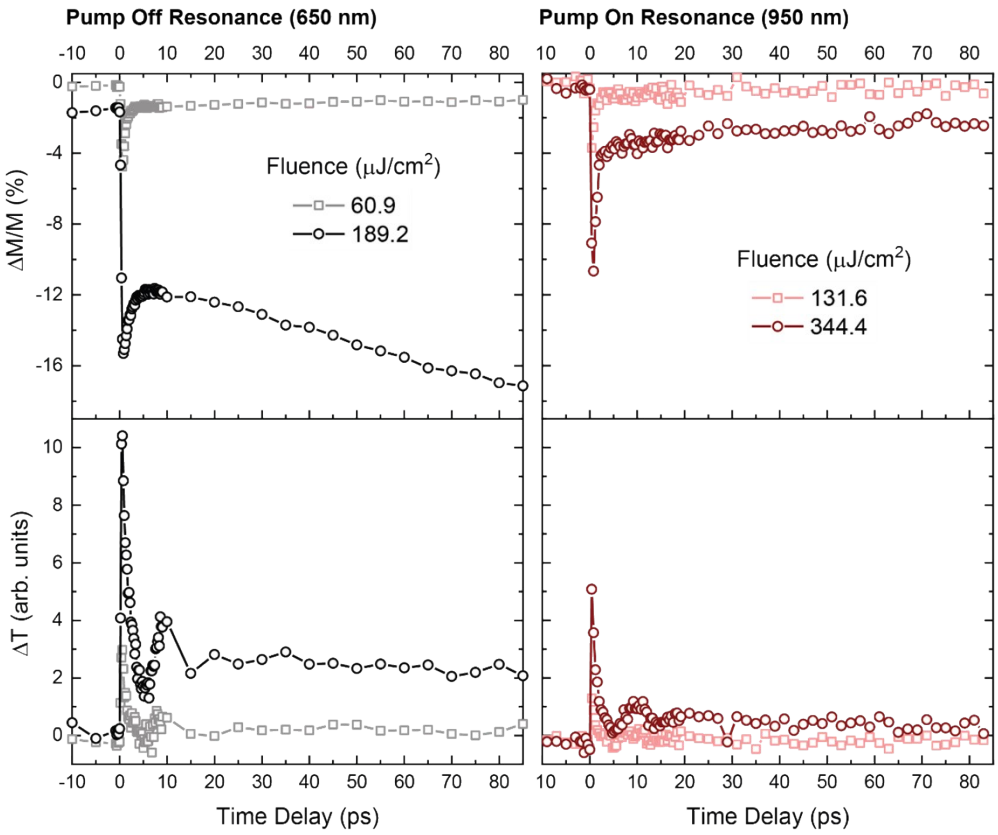

Figure S2. Long time-scale magnetization (top panels) and transmission (bottom panels) dynamics of the nanorings + ferrimagnet system for off-resonance (left panels) and on-resonance (right panels) excitation. Transmission dynamics show oscillations corresponding to a standing acoustic wave excited in the 20 nm thick $Tb_{26}Co_{74}$ film.

S3: Details of experimental setup:

Transmission spectra: Optical transmission spectra were measured using a commercial Agilent Cary 60 UV-vis spectrophotometer.

Pump-Probe Spectroscopy: A representative schematic setup of a typical pump-probe setup is shown in Figure S3.2. The pump and probe beams are derived from a Spectra-Physics Spitfire Ti-Sapphire amplified laser system with a repetition rate of 1 kHz and a central wavelength of 800

nm. The 800nm output is used as a probe, whereas the pump is derived by passing the 800nm output through an Optical Parametric Amplifier (Spectra-Physics TOPAS) to obtain either 650 nm or 950 nm. The pump and probe beams have been aligned so as the temporal overlap of the two beams on the sample occurs within the range of motion of a commercial delay stage. The pump is modulated using a mechanical chopper operated at 500 Hz such that every alternate pump beam is blocked. In this way, pump-induced changes can be extracted from the modulated probe signal using a lock-in amplifier. Combinations of half wave plates and polarizers are used to fine tune the incident powers of the pump and probe beams. Converging lenses are used to focus the beams on the sample and the spatial overlap between the pump and probe beams is optimized using mirrors. The sample is placed between two poles of a standard electromagnet, the field output of which can be varied using an external, programmable current supply. The probe beam transmitted through the sample is directed to a pair of balanced Si-photodiodes, allowing measurement of pump-induced changes in transmitted intensity as well as polarization rotation. The pump beam is blocked from entering the detector using suitable colour filters.

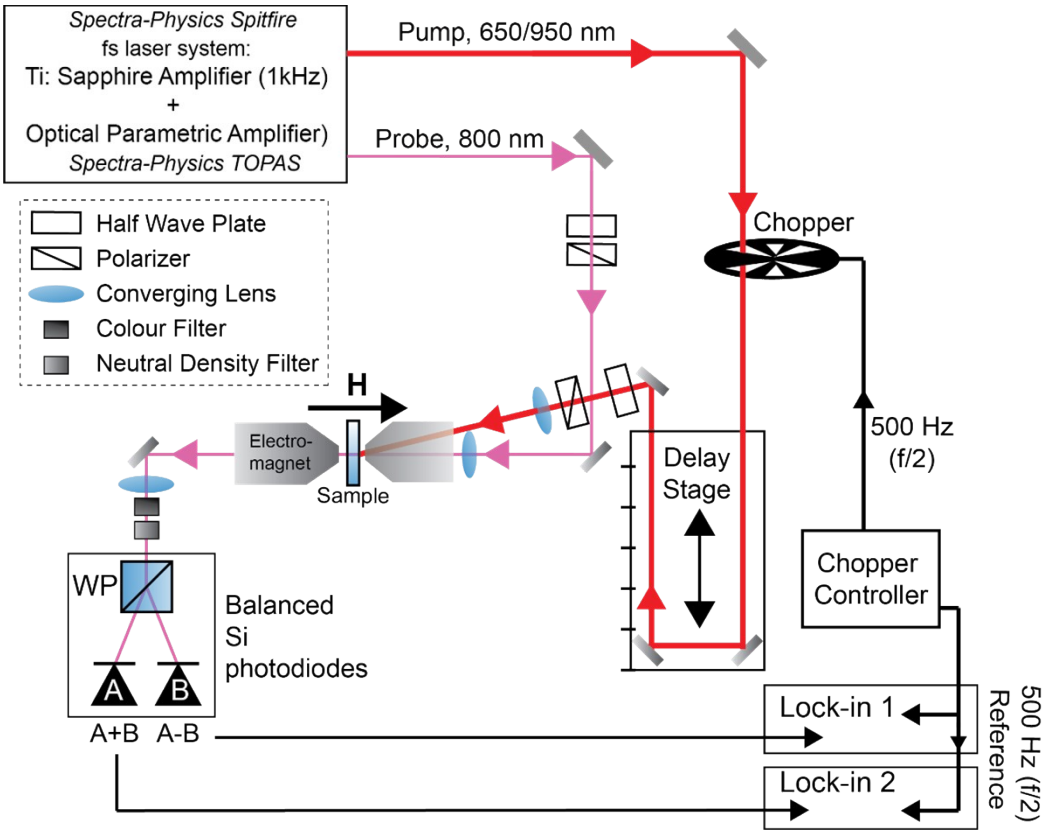

Figure S3.2 Representative schematic of the pump-probe setup used to measure the transmission and magnetization dynamics traces

REFERENCES:

37. A. Mekonnen *et al.*, "Role of the inter-sublattice exchange coupling in short-laser-pulse-induced demagnetization dynamics of GdCo and GdCoFe alloys", *Phys. Rev. B* 87.18 (2013), p 180405.

38. P. E. Hopkins, M. Ding, and J. Poon, "Contributions of electron and phonon transport to the thermal conductivity of GdFeCo and TbFeCo amorphous rare-earth transition-metal alloys", in *Journal of Applied Physics*, 111.10 (2012) p. 103533.